A&A 411, L179–L183 (2003)
DOI: 10.1051/0004-6361:20031584

Astronomy & Astrophysics

The INTEGRAL IBIS/ISGRI System Point Spread Function and Source Location Accuracy⋆

A. Gros[1], A. Goldwurm[1], M. Cadolle-Bel[1], P. Goldoni[1], J. Rodriguez[1,5], L. Foschini[2], M. Del Santo[3], and P. Blay[4]

[1] CEA Saclay, DSM/DAPNIA/SAp, 91191 Gif-sur-Yvette Cedex, France
[2] IASF/CNR, sezione di Bologna, via Gobetti 101, 40129 Bologna, Italy
[3] IASF/CNR, sezione di Roma, via del Fosso del Cavaliere 100, 00133 Roma, Italy
[4] GACE, Instituto de Ciencia de los Materiales, Universidad de Valencia, PO Box 22085, 46071 Valencia, Spain
[5] Integral Science Data Center, Chemin d'Écogia 16, 1290 Versoix, Switzerland

Received 18 July 2003 / Accepted 9 October 2003

Abstract. The imager on board INTEGRAL (IBIS) presently provides the most detailed sky images ever obtained at energies above 30 keV. The telescope is based on a coded aperture imaging system which allows to obtain sky images in a large field of view ($29^\circ \times 29^\circ$) with an angular resolution of $12'$. The System Point Spread Function of the telescope and its detailed characteristics are here described along with the specific analysis algorithms used to derive the accurate point-like source locations. The derived location accuracy is studied using the first in-flight calibration data on strong sources for the IBIS/ISGRI system. The dependence of the calibrated location accuracy with the signal to noise ratio of the sources is presented. These preliminary studies demonstrate that the IBIS/ISGRI telescope and the standard scientific analysis software allow source localizations with accuracy at 90% confidence level better than $1'$ for sources with signal to noise ratios >30 over the whole field of view, in agreement with the expected performances of the instrument.

Key words. methods: data analysis – techniques: image processing – techniques: high angular resolution

1. Introduction

The IBIS telescope (Imager on Board of the INTEGRAL Satellite) (Ubertini et al. 2003), launched onboard the major ESA gamma-ray space mission INTEGRAL (Winkler et al. 2003) on October 2002, is a hard X-ray/soft γ-ray telescope based on a coded aperture imaging system (Goldwurm et al. 2001). The IBIS imaging system and the IBIS scientific data analysis are described in Goldwurm et al. (2003). Here we discuss more in detail the specific image data analysis procedures used to evaluate the point source locations and we present the characteristics of the System Point Spread Function obtained with the implemented analysis. We also provide preliminary results on the source location accuracy obtained from the first in-flight calibration data of ISGRI, the low energy (15–1000 keV) detector of IBIS (Lebrun et al. 2003).

Send offprint requests to: A. Gros,
e-mail: Aleksandra.Gros@cea.fr

⋆ Based on observations with INTEGRAL, an ESA project with instruments and science data centre funded by ESA member states (especially the PI countries: Denmark, France, Germany, Italy, Switzerland, Spain), Czech Republic and Poland, and with the participation of Russia and the USA.

2. The IBIS image decoding and the associated System Point Spread Function

In coded aperture telescopes (Dicke 1968; Fenimore & Cannon 1981; Caroli et al. 1987; Goldwurm 1995), the source radiation is spatially modulated by a mask of opaque and transparent elements before being recorded on a position sensitive detector. Reconstruction of the sky image is generally based on a correlation procedure between the recorded image and a decoding array derived from the mask pattern. For the IBIS system, where the mask is built by the replication of a Modified Uniformly Redundant Array (MURA) basic pattern (Gottesman & Fenimore 1989) of the size of the detection plane, the raw image projected on the detector by a source in the Fully Coded Field of View (FCFOV) (sky region from where the recorded source radiation is fully modulated by the mask) will be a shifted version of the mask basic pattern. A source in the Partially Coded FOV (PCFOV) will instead project only a part of the mask pattern. The total recorded image (the shadowgram) is therefore the sum of the shadows projected by all sources in the FOV plus a background term. For those masks patterns for which a *correlation inverse matrix* exists, the case of the IBIS system (Goldwurm et al. 2003), the sky image is reconstructed by correlation of the shadowgram with a decoding array obtained from its correlation inverse matrix (Fenimore & Cannon 1981). For those systems (and with a

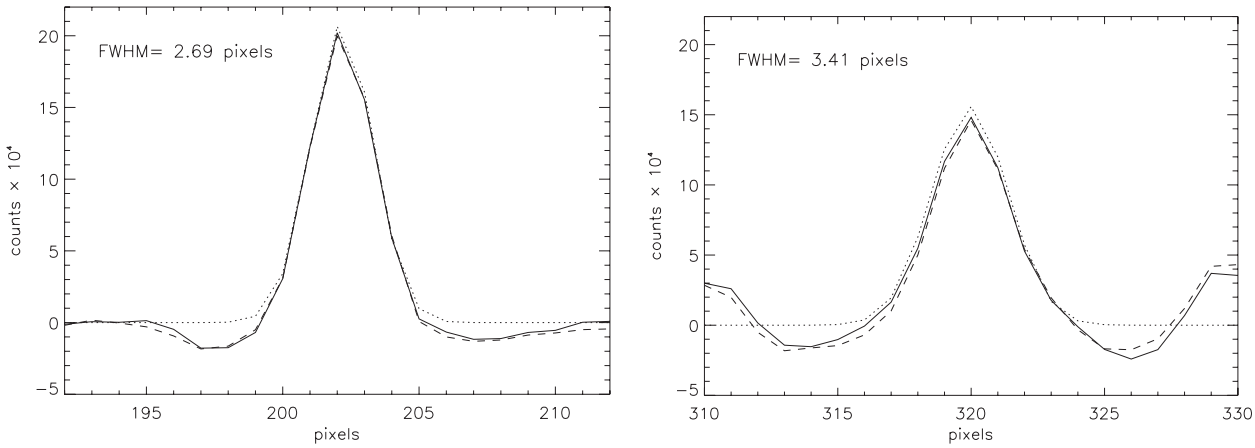

Fig. 1. The ISGRI SPSF compared to the analytical approximation used to fit source positions in the FCFOV (left) and in the PCFOV (right). The reconstructed source profiles (solid line) before normalization to the FCFOV for the Crab and the fitted bidimensional Gaussians (dotted line) are shown (fitted FWHM are 2.69 pixels for the FCFOV and 3.41 pix for the PCFOV). Also shown is the source model profile (broken line) computed at the position derived from the Gaussian fit.

perfect detector) the resulting sky image of a single point-like source in the FCFOV will have a main peak at the source position, flat side lobes in the FCFOV and coding noise with 8 main source ghosts in the PCFOV. For a PCFOV source, a main peak will still be present at the source position but coding noise can extend all over the image starting from the close proximity of the main peak and ghosts will appear in the FOV. The distribution of the coding noise does depend on the mask pattern used. For example URA masks built from quadratic residues (Fenimore & Cannon 1981) have a high degree of symmetry along the axis of the mask, unlike those built from Hadamard arrays (Proctor et al. 1979). This leads the coding noise to concentrate along the image axis passing through the source main peak, producing positive and negative sidelobes (see Fig. 3 in Goldwurm et al. 2003).

We refer to the System Point Spread Function (SPSF) as the spatial response of the system to a point-like source *after* image deconvolution, i.e. considering the decoding process (Fenimore & Cannon 1981). We will discuss here the SPSF relative to the type of deconvolution described in Goldwurm et al. (2003), used in the IBIS standard data analysis and optimized to obtain the best signal to noise (S/N) for point-like sources. This is basically a kind of balanced finely sampled cross correlation (Fenimore & Cannon 1981) extended to the PCFOV (Goldwurm 2001; Goldwurm et al. 2003) and in which the sampling of the decoding array is performed in such a way to weigh the detector pixels with the fraction of transparent or opaque area projected by the mask elements (Sect. 3).

The algorithm implemented is fully described in Sect. 2 of Goldwurm et al. (2003). From the mask array M (=0 for opaque elements and =1 for transparent elements) two decoding array G^+ and G^- are obtained projecting the arrays M and $1-M$ over a detector pixel grid and padding the zones outside the mask with 0s. Then the sky image S is derived from the detector image D by appling the following operation for each i, j sky pixel and where sums run over all k, l detector pixels

$$S_{ij} = \sum_{kl} G^+_{i+k,j+l} W_{kl} D_{kl} - B_{ij} \sum_{kl} G^-_{i+k,j+l} W_{kl} D_{kl}$$

where $B_{ij} = \frac{\sum_{kl} G^+_{i+k,j+l} W_{kl}}{\sum_{kl} G^-_{i+k,j+l} W_{kl}}$ is the balance array and the array W is set to 0 for dead or noisy pixels and to 1 for active good pixels. The correlation performed is balanced in the sense that in absence of sources and with a constant background term, the reconstructed images are flat. The decoded images are then properly renormalized to the reconstructed counts in the FCFOV.

The above deconvolution for a perfect URA coded mask system would provide for a source in the FCFOV a SPSF close to a pyramidal function with totally flat sidelobes in the FCFOV (Fenimore & Cannon 1981). However since the coding is not perfect, due to several instrumental effects like those produced by dead zones between pixels and detector modules and by the supporting structures, the reconstructed image will contain source sidelobes. In the PCFOV sidelobes are inherent to the decoding process even for a perfect detector system and the reconstructed source peak for this decoding procedure can be larger or distorted because of the imperfect coding (Sect. 4). Because of the presence of the ghosts and of the coding noise, the general sky image reconstruction process is an iterative procedure that combine the initial decoding process to the analysis, modelling and cleaning of sidelobes for each source detected in the field. In crowded fields the initial source localization may be disturbed by the presence of other source sidelobes, but as the modelling of the sky is improved during the iterations the localization can improve. However the performances of the localization in this case depends on the number and distribution of sources in the FOV and the performances of the iterative procedure including the convergence criteria used. We present here the characteristics of the SPSF at the first step of the iterative procedure after the first decoding and before the sidelobe cleaning, and we focus on the characteristics of the main peak of the SPSF around the source position.

The main peak angular width will be approximately of the projected angular size of the mask element, i.e. for the IBIS telescope $\approx 12'$ (FWHM). However the exact shape of the SPSF depends also on the detector spatial resolution, the real features of the telescope (e.g. presence of dead and off-pixel zones, mask thickness, etc.) and on the decoding algorithm.

3. Analytical approximation and fitting procedure of the SPSF

The pixels of the IBIS detectors are smaller than the mask elements. The ratio R of the linear mask element size to the linear pixel size is 2.43 for ISGRI. In order to better sample the shadowgram, the corresponding decoding array is also sampled at the pixel scale by redistributing its values according to the fraction of pixel area covered by a given projected mask element. The resulting decoded image has pixels of the angular size of the detector pixels (≈4.94′). This way of sampling the decoding array before deconvolution optimizes the signal to noise ratio of point-like sources in the reconstructed image, as it takes into account the blurring induced by the finite spatial resolution of the detector (discrete pixels) (Cook et al. 1984).

For this reconstruction the theoretical SPSF peak in the FCFOV is space-invariant and given by the convolution of two square-pyramidal functions with FWHM's equal to $w_{\rm m}$, mask element size, and $w_{\rm p}$, linear pixel size, respectively. Using the central limit theorem we see that the convolution of these functions can be approximated by a bi-dimensional Gaussian with a width of $w_{\rm spsf} \approx \sqrt{w_{\rm m}^2 + w_{\rm p}^2}$. For IBIS/ISGRI, using pixel units, $w_{\rm p} = 1$, $w_{\rm m} = 2.43$, $w_{\rm spsf} = 2.62$. This is slightly worse than the theoretical angular resolution of one projected mask element $w_{\rm m}$. The standard imaging analysis procedure of the IBIS data performs, for each detected significant excess in the deconvolved image, a χ^2 fit between an image sector around the source peak and a bi-dimensional Gaussian. The free parameters are the centroid position of the Gaussian (2 parameters), the 2 (variable in PCFOV) widths along the 2 axis, the amplitude of the Gaussian and a constant level (background).

In Fig. 1 we show the reconstructed peak of a strong point-like source for the IBIS/ISGRI system, versus the best fitted bi-dimensional Gaussian, in both the FCFOV (left) and the PCFOV (right). The source is the well known Crab (nebula and pulsar) which was observed with INTEGRAL in February 2003. The best fit Gaussian width is about 2.65 pixels which is compatible with $w_{\rm spsf}$. A bi-dimensional Gaussian function is a reasonable approximation of the SPSF peak except for the negative wings around the source, due to the non perfect coding of the detector plane (in the FCFOV mainly due to the dead zones). These side lobes will be corrected using the source model once its fine position is determined. Figure 1 shows also the shape of the peak obtained from the deconvolution of the source model computed a posteriori for the position obtained with the Gaussian fit. One can see that the SPSF shape (including the wings) is well reproduced by the model. However, the computation of such a model and its deconvolution is time consuming and thus difficult to use for fine determination of the source position. The source location is therefore determined by a fitting procedure with a Gaussian function and the errors by the standard computation involving the curvature matrix (Press et al. 1996). The error computation assumes Gaussian distribution of the counts and also independence between pixels. In such decoded image the sky pixels are instead highly correlated in particular on length scales of the mask elements. Moreover the residual background structures may make the distribution

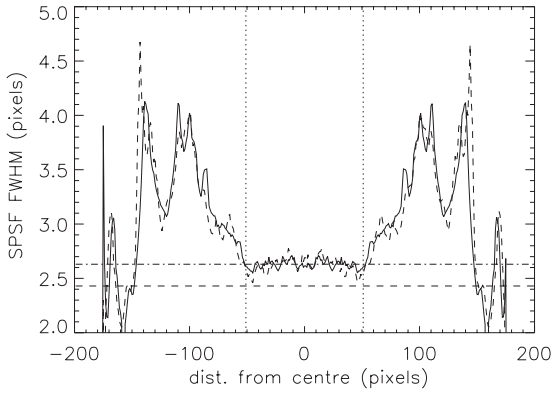

Fig. 2. The variation of the width of the SPSF (for the adopted decoding and before sidelobe cleaning) along the FOV of the IBIS/ISGRI telescope, for the two axis (solid line for the Y axis and broken line for the Z axis). The two horizontal lines indicate the widths $w_{\rm m}$ and $w_{\rm spsf}$ and the two dotted vertical lines the limits of the FCFOV.

highly non-Gaussian. While the optimization procedure is still valid, the derived goodness of the fit and error determination may suffer of these conditions. The computed formal statistical error can be underestimated and systematic errors may be dominant, therefore it is important to evaluate the uncertainties using in-flight data and studying the systematic effects in the procedure.

4. The shape of the SPSF in the PCFOV

Outside the FCFOV the SPSF is not space invariant even if the detector plane were perfect, because the optimum properties of the MURA mask are not respected. The shape of the SPSF we obtain for the decoding process applied can be distorted or enlarged (Fig. 1, right). We have studied the properties of the SPSF in the total FOV of the telescope and the performances and limitations of the Gaussian fitting procedure using the source model. Figure 2 shows the fitted width of the SPSF on both axis for source positions all along the FOV. The width is approximately constant in the FCFOV and ranges around 2.6. In the PCFOV however it increases up to values of about 4 pixels (≈20′). The behavior is symmetric with respect to the image center and similar along the two axis. As a consequence off-axis sources can appear elongated or spread in the reconstructed images.

By studying the offset between the fitted and input source model position, we have derived a measure of the systematic bias introduced by the approximation made for the form of the SPSF. The effect is not large (<0.5′) and can be estimated. An automatic correction of the bias has been included in the localization procedure. From the first analysis of in flight IBIS/ISGRI data, a systematic offset between the IBIS telescope axis and the axis of the satellite star sensors used to reconstruct the absolute spacecraft attitude was found. This predominant (≈8′–10′) effect, was measured using the localization procedure described here and the available INTEGRAL data. A matrix for misalignement correction was computed (Walter et al. 2003) and included in the localization algorithms which operate the conversion between sky pixels and celestial

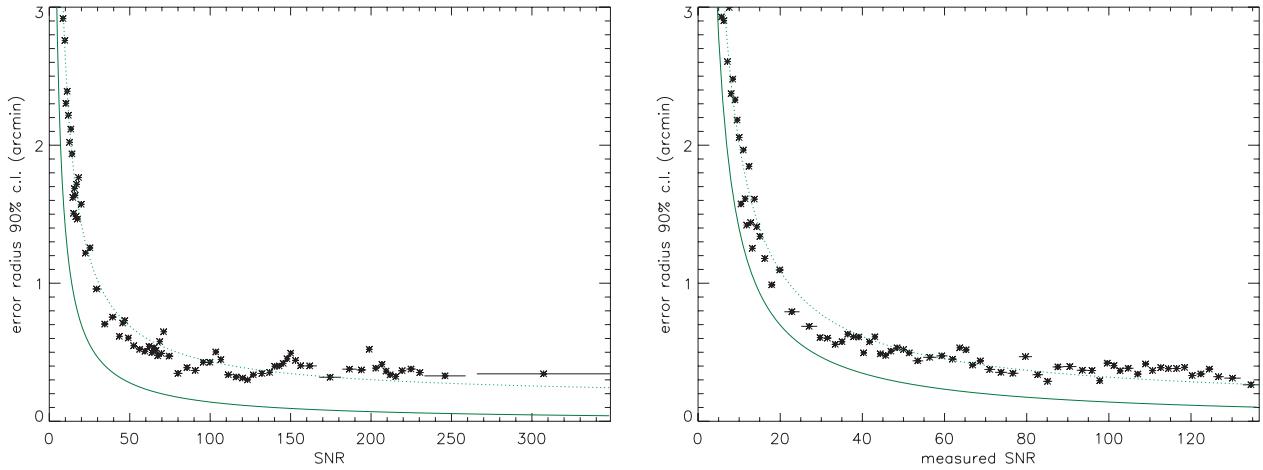

Fig. 3. The 90 % confidence level (c.l.) error radius on the point-like source location of the IBIS/ISGRI telescope vs. the source signal to noise ratio (S/N), as derived from in-flight calibrations. S/N bins include 30 measures of the offset. The values are compared to the theoretical 90% c.l. PSLE (solid line). The plotted data were fitted with a function of the type $y = ax^c + b$ (broken line). *Left*: values derived from ∼2000 offset measures of reconstructed Crab, Cyg X-1 and Cyg X-3 locations in energy bands between 20 and 300 keV, with source positions ranging between 0° and 14° from the telescope axis. The best fit parameters are $a = 22.1$, $b = 0.16$ and $c = -0.95$. *Right*: Same values plotted versus a *measured* S/N (see text).

coordinates. The imaging software has already provided good results for the source absolute positioning with IBIS/ISGRI data (see this volume for a number of results).

In the following we characterize the performance of the system (the telescope and the software) in term of the point source location accuracy obtained with the most recent version of the IBIS/ISGRI specific analysis software that will be implemented in the October 2003 release of the ISDC Off-line Scientific Analysis (OSA 3.0). The location algorithms have been improved and provide now location accuracies for off-axis sources comparable to those of on-axis sources, therefore with better results than previously reported (Walter et al. 2003).

5. The IBIS point source location error

From the formal errors computed through the curvature matrix, it can be shown that the average Point Source Location (statistical) Error (*PSLE*) for an optimum coded aperture system with a defined *SPSF* depends on the source signal to noise ratio (*S/N*) as $PSLE \div \frac{1}{R \times (S/N)}$. The *S/N* is the ratio between the reconstructed source peak and the computed statistical standard deviation associated to the peak pixel. Using computation of such error and simulations performed on a *perfect system* with the geometrical characteristics of the IBIS/ISGRI telescope, we derived the expected PSLE dependence on the *S/N* (Goldwurm et al. 2001). This curve represents the best theoretical accuracy of point-like source location which can be attained by such a system.

With the described analysis software we have derived the locations of several strong known sources, for different pointings and energy bands. This has provided us with a number of measured source locations in a wide range of S/N ratios and angles from the telescope axis. We have computed the offsets between the derived and catalogue source positions and compared their 90% confidence level dispersion to the theoretical PSLE values. Figure 3 (left) shows the results obtained combining all measures performed for source $S/N \geq 6$. The S/N bin widths were defined to include a constant number of measured offset values, in order to have similar precision in each bin. Sources at any distance from the telescope axis were measured and no dependence with axis angle or energy is observed. It can be seen that measured offsets are typically comprised between 3′ and 20″ and are better than 1′ for $S/N > 30$. Although the points do not exactly follow the theoretical PSLE curve, there is a clear trend compatible with the expected dependence on *S/N* (see derived parameters in Fig. 3). At high S/N the dispersion reaches a constant level of about 20″ which shows the maximal accuracy obtained. Residual systematic effects (for example due to background structures) may still influence the dispersion, and work is in progress to fully evaluate their impact on the source location determination.

In Fig. 3 (right) we report the error radius versus a *measured* S/N rather than the pure statistical *S/N*. The measured S/N is obtained using a standard deviation computed directly from the reconstructed sky image. In our analysis we measured the standard deviation in a region of 2.5° × 2.5° around the source after cleaning the side lobes of all sources detected in the FOV and neglecting the source peak regions. This way to evaluate the S/N includes an estimate of the residual systematic errors. The derived offsets are now much closer to the theoretical PSLE curve and indicate that an even better evaluation of location error may be obtained when systematic effects will be fully accounted for.

We stress that these results involve fields with few detected sources. For crowded fields the location estimate may depend on the efficiency of the iterative cleaning algorithm and a full detailed evaluation is not yet available. On the other hand, we have verified that the location accuracy obtained by applying the same algorithm and approximation of the SPSF to mosaicked images (Goldwurm et al. 2003) is further improved. The results we have obtained for selected sources in combined images show that their localization indeed improves for a given

statistical S/N. This may be due to the fact that the systematic effects present in single pointings are smoothed when images are summed. Using Cyg X-1 data, offsets of the order of 5″–10″ have been obtained for S/N values >300.

These results show that the IBIS/ISGRI telescope coupled to the analysis procedures we have developed provide point-like source locations with accuracies which fully comply with the expected performance of the instrument.

Acknowledgements. A. Gros and J.R. acknowledge financial support from the French Space Agency (CNES). L.F. and M.D.S. acknowledge financial support from the Italian Space Agency (ASI) and the hospitality of the ISDC.

References

Caroli, E., Stephen, J. B., Di Cocco, G., Natalucci, L., Spizzichino, A. 1987, Space Sci. Rev., 45, 349
Cook, W. R., Finger, M., Prince, T. A., & Stone, E. C. 1984, IEEE Trans. Nucl. Sci., NS-31, 771
Dicke, R. H. 1968, ApJ, 153, L101
Fenimore, E. E., & Cannon, T. M. 1978, Appl. Opt., 17(3), 337
Fenimore, E. E., & Cannon, T. M. 1981, Appl. Opt., 20(10), 1858
Goldwurm, A. 1995, Exper. Astron., 6, 9
Goldwurm, A., Goldoni, P., Gros, A., et al. 2001, Proc. of the 4th INTEGRAL Workshop, ed. A. Gimenez, V. Reglero, & C. Winkler, ESA-SP, 459, 497
Goldwurm, A., David, P., Foschini, L., et al. 2003, A&A, 411, L223
Gottesman, S. R., & Fenimore, E. E. 1989, Appl. Opt., 28, 4344
Lebrun, F., Leray, J.-P., Lavocat, P., et al. 2003, A&A, 411, L141
Press, W. H., Teukolsky, S. A., Vellerling, W. T., Flannery, B. P. 1992, Numerical Recipes (Cambridge, Cambridge University Press)
Proctor, R. J., Skinner, G. K., & Willmore, A. P. 1979, MNRAS, 187, 633
Ubertini, P., Lebrun, F., Di Cocco, G., et al. 2003, A&A, 411, L131
Walter, R., Favre, P., Dubath, P., et al. 2003, A&A, 411, L25
Winkler, C., Courvoisier, T. J.-L., Di Cocco, G., et al. 2003, A&A, 411, L1